analytical chemistry

pubs.acs.org/ac Article

Spatiotemporal Characterization of GPCR Activity and Function during Endosomal Trafficking Pathway

Hyunbin Kim, Hae Nim Lee, Jaesik Choi,* and Jihye Seong*

Cite This: *Anal. Chem.* 2021, 93, 2010−2017 Read Online

ACCESS | Metrics & More | Article Recommendations | Supporting Information

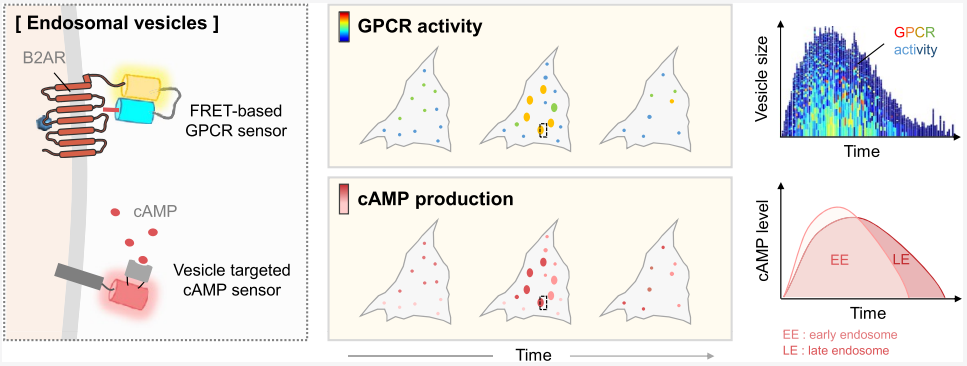

ABSTRACT: G protein-coupled receptor (GPCR) is activated by extracellular signals. After their function at plasma membrane, GPCRs are internalized to be desensitized, while emerging evidence suggests that some GPCRs maintain their activity even after internalization. The endosomal trafficking pathway of a prototypic GPCR, β adrenergic receptor 2 (B2AR), is in the range of several hours, however, spatiotemporal B2AR activity during this long-term endosomal trafficking pathway has not been characterized yet. Here, we analyze an agonist-induced real-time B2AR activity and its downstream function at the level of individual vesicles, utilizing a fluorescence resonance energy transfer (FRET)-based B2AR biosensor and cAMP reporters tethered at different trafficking stages of endosomes. Our results report that the internalized B2ARs sustain the activity and maintain the production of cAMP for several hours during the endosomal trafficking pathway. Temporal kinetics of B2AR activity is mathematically well explained by our active-vesicle population model modified from the Ricker model. Therefore, our GPCR monitoring system and a new kinetics model can be applied to understand the spatiotemporal GPCR activity and its downstream function during the endosomal trafficking pathway.

G protein-coupled receptors (GPCRs) receive various extracellular signals and initiate diverse intracellular responses through the interactions with heterotrimeric G proteins at plasma membrane.[1,2] Activated GPCRs are further phosphorylated by G-protein-coupled receptor kinases (GRKs) recruiting β-arrestins and then internalized from plasma membrane.[3,4] This internalization process was suggested as a major termination mechanism of GPCR signaling pathways.[4,5]

However, emerging evidence suggests that some GPCRs can sustain their activity even after internalization and mediate their downstream G-protein signaling at endosomes.[6−8] For example, the internalized thyroid-stimulating hormone (TSH) receptor continues to mediate its G-protein signaling producing cAMP via adenylyl cyclase (AC).[9] Other GPCRs exhibiting sustained signaling include parathyroid hormone receptor (PTHR),[10] sphingosine 1-phosphate receptor 1 (S1PR1),[11] β-adrenergic receptor 2 (B2AR),[12] glucagon-like peptide receptor 1 (GLP1R),[13] and vasopressin receptor 2 (V2R).[14]

In particular, it has been directly visualized by a nanobody-based biosensor Nb80-GFP that B2AR, a prototype GPCR, maintains the active conformational state at the internalized endosomes generating cAMP.[12] Interestingly, this endosomal cAMP level is shown to be required for cAMP-dependent transcription control,[15] implying spatial encoding of cAMP signaling pathway. Indeed, compartmentalized cAMP signals are revealed by real-time cAMP imaging with fluorescent protein (FP)-based sensors.[16] A recent study reports that adenylyl cyclase type 9 (AC9), the G protein effector that generates cAMP, can be trafficked from plasma membrane to endosomes,[17] supporting the sustained endosomal GPCR signaling pathway after internalization.

Received: August 5, 2020
Accepted: December 18, 2020
Published: January 5, 2021

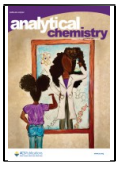

https://dx.doi.org/10.1021/acs.analchem.0c03323
Anal. Chem. 2021, 93, 2010−2017

After internalized from plasma membrane, GPCRs at early endosomes are quickly recycled back to the cell surface (short-term desensitization), while in a prolonged presence of agonist, they are trafficked to late endosomes and then combined with lysosomes to be eventually degraded (long-term desensitization).[18−20] During the long-term desensitization, the endosomal trafficking pathway of B2AR is dependent on ubiquitin and ESCRT (endosome sorting complex required for transport) complex, which suggested to be in the range of several hours.[21−24] Despite this long-term B2AR trafficking pathway, previous studies focused on early response of endosomal B2AR activity and signaling within an hour.[9,12,15] However, spatiotemporal B2AR activity and signaling for several hours are not yet characterized throughout the whole endosomal trafficking pathway, which is crucial for the strength and duration of its cellular function.[25]

To monitor the long-term B2AR activity during the endosomal trafficking pathway, we apply a genetically encoded B2AR biosensor based on fluorescence resonance energy transfer (FRET).[26] Because the C-terminus of B2AR is crucial for its trafficking process,[3,27,28] this FRET biosensor contains the full B2AR sequence and after its C-terminus, the FRET sensing domains are linked by flexible $(GSS)_4$ sequences. To measure the B2AR-mediated cAMP production during the endosomal trafficking pathway, we targeted a genetically encoded cAMP indicator[29] to different trafficking stages of endosomes. Finally, we developed an endosome-tracking program to accurately analyze the spatiotemporal B2AR activity as well as its downstream function at the level of endosomal vesicles.

Utilizing these systems, we characterize an agonist-induced B2AR activation and the subsequent production of cAMP during the endosomal trafficking pathway and long-term desensitization. After a rapid B2AR activation at plasma membrane in a few minutes, the internalized B2AR at endosomal vesicles maintains its activity for several hours, mediating local production of cAMP during the endosomal trafficking pathway. We mathematically explain the kinetics of the endosomal B2AR activity by our active-vesicle population model. Therefore, we report the spatiotemporal B2AR activity and function throughout the whole endosomal trafficking pathway in live cells.

EXPERIMENTAL SECTION

Plasmids. FRET-based B2AR biosensor has been previously described.[26] To improve its localization at plasma membrane, a signal peptide sequence from hemagglutinin (HA)[30] and a FLAG epitope were further inserted at the N-terminal of the biosensor by PCR and In-Fusion (Clontech) techniques. A B2AR-pH sensor was generated by replacing fluorescent proteins (mCerulean to pHTomato, mCitrine to EGFP) in pcDNA5 vector. To create subcellular cAMP indicators, Rab5a or Rab7a was fused to the C-terminal of pink Flamindo (pF),[29] and LAMP2B was inserted in the N-terminus of pF. Full sequences of new constructs are available in the Supporting Material. pTagBFP-Rab5a, TagRFP-T-EEA1, GFP-Rab7a, LAMP-1-mGFP, LAMP2B, mScarlet-C1, and pink Flamindo were obtained from Addgene.

Cell Culture and Transfection. Human embryonic kidney 293A (HEK293A) cell line was maintained in Dulbecco's modified Eagle's medium (DMEM) supplemented with 10% fetal bovine serum (FBS, Hyclone), 1 unit per mL penicillin, 100 μg per mL streptomycin, and 100 μM MEM Non-Essential Amino Acids Solution (Gibco). Starvation media contains reduced FBS (0.5%). Cells were cultured in a humidified 95% air and 5% CO_2 incubator at 37 °C. Lipofectamine 2000 reagent (Invitrogen) was used for transfection according to the manufacturer's protocol. Isoproterenol hydrochloride was purchased from Tocris.

Image Acquisition. Images were collected by a Nikon Ti-E inverted microscope and a cooled charge-coupled device camera using NIS software (Nikon). FRET images were collected using a 438DF24 excitation filter, a 458DRLP dichroic mirror, and two emission filters controlled by a filter changer (483DF32 for CFP and 542DF27 for FRET). For the FRET measurement, the CFP and FRET images at each time point were collected with an exposure time of 200 ms with a neutral density (ND) 8 filter. The fluorescence intensity of nontransfected cells was quantified as the background signals and subtracted from that of transfected cells. The pixel-by-pixel FRET/CFP ratio images were calculated based on the background-subtracted fluorescence intensity images of CFP and FRET by the NIS program.

Live-Cell Imaging. Live-cell imaging was performed in a humidified 95% air, 5% CO_2, and 37 °C temperature-controlled chamber (Live Cell Instrument). HEK293A cells expressing B2AR biosensor or other constructs were prepared on cover-glass-bottom dishes (SPL Life Sciences) coated with 10 μg/mL of fibronectin (Invitrogen) and starved overnight under 0.5% FBS-containing starvation media. On the day of live-cell imaging, isoproterenol (10 μM) was added to the cells for 10 min, and the media was replaced with new starvation media. Cells were monitored on the 100× objective lens, and the images were taken every 5 or 10 min.

Computational Analysis. Each individual vesicle was identified by watershed algorithm, and the FRET/CFP level of the B2AR biosensor at each endosomal vesicle was analyzed with our homemade program based on openCV library.[31] To improve the accuracy of vesicle detection, the program finds a set of local maxima where each maximum point is separated from another maximum point by a specified distance. When the mean intensity of a detected vesicle is lower than a threshold, the program discards the vesicle from consideration. The threshold was adjusted since images of different cells have different distributions of activation and intensity levels. The intensity was computed from the FRET/CFP ratio image using the coordinates of vesicles extracted from the paired CFP image.

The parameters (α, r, c, and k) of our population model are learned by the gradient descent method implemented in TensorFlow.[32] The parameter is determined by minimizing the difference between our predicted populations and measured populations. Our model can also be represented by a polynomial term multiplied with an exponential term as follows (eq 1)

$$a_{t+1} = a_0 \times \prod_{i=1}^{t} c \times \left(1 + \frac{1}{i}\right)^{\alpha} \exp\left(r\left(1 - \frac{A_i}{k}\right)\right)$$

$$= a_0 \times \prod_{i=1}^{t} c \times \left(\frac{i+1}{i}\right)^{\alpha} \exp\left(\sum_{i=1}^{t} r\left(1 - \frac{A_i}{k}\right)\right)$$

$$= a_0 \times c^t \times (t+1)^{\alpha} \exp\left(rt - \frac{r}{k}\sum_{i=1}^{t} A_i\right)$$

https://dx.doi.org/10.1021/acs.analchem.0c03323
Anal. Chem. 2021, 93, 2010−2017

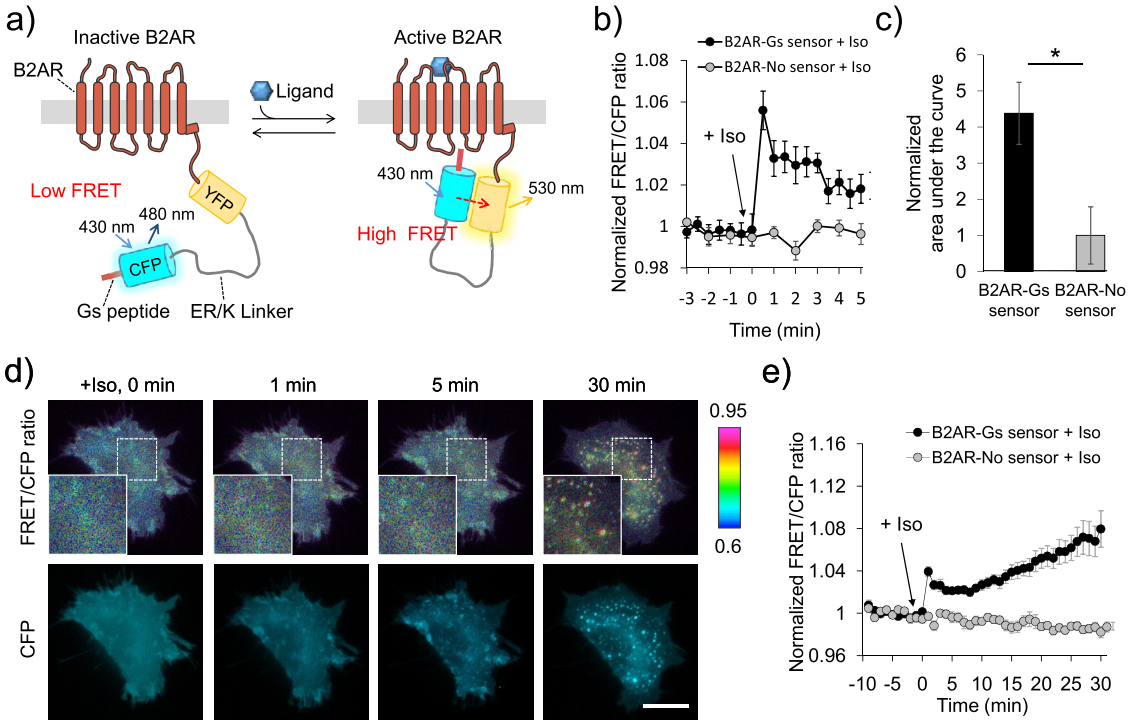

Figure 1. FRET-based B2AR biosensor detects a rapid activation of B2AR at plasma membrane and the subsequent internalization. (a) Scheme of the B2AR-Gs FRET biosensor. (b) Time course of the normalized FRET/CFP emission ratio of B2AR-Gs biosensor or B2AR-No biosensor (a negative control sensor without the C-terminal sequence derived from Gs protein) in response to the treatment of 10 μM Isoproterenol (Iso) for indicated times. Data represent the mean value ± s.e.m. (n = 10, n represents the number of individual cell experiments). (c) Area under the curve of B2AR-Gs biosensor or B2AR-No biosensor was calculated from 0 to 5 minutes after Iso treatment. Normalization was performed by B2AR-No biosensor as a 1. * represents significant difference between groups (p = 0.0015). (d) FRET/CFP ratio (top) and CFP images (bottom) of the B2AR biosensor after the Iso treatment for indicated times. High magnified FRET/CFP ratio images are presented in the inserted boxes (top). The rainbow color bar on the top right represents the level of FRET/CFP emission ratio. Scale bar, 20 μm. (e) Time course of the normalized FRET/CFP emission ratio of B2AR-Gs biosensor (n = 11) and B2AR-No biosensor (n = 16) after the Iso treatment. Data represent the mean value ± s.e.m.

Thus, a_t can be represented as

$$a_t = a_0 \times c^t \times t^\alpha \times \exp\left(rt - \frac{r}{k}\sum_{i=1}^{t-1} A_i - r\right) \quad (1)$$

Statistical Analysis. To determine the p values between experimental and control groups, a statistical analysis was performed using a two-tailed Student's t-test at Origin2017 or Excel, and the values are shown as mean ± standard error of the mean (s.e.m.) for control and experimental samples (*p < 0.05).

RESULTS AND DISCUSSION

FRET-Based Visualization of Agonist-Induced Rapid B2AR Activation at Plasma Membrane. To detect the real-time B2AR activity during agonist-stimulated endocytosis, we utilized a genetically encoded B2AR biosensor based on fluorescence resonance energy transfer (FRET).[26] This FRET-based B2AR biosensor is composed of full sequence of B2AR, $(GSS)_4$ linker, yellow fluorescent mCitrine, ER/K linker, cyan fluorescent mCerulean, and the 27 C-terminal residues from Gαs protein (Figure 1a). An agonist-induced conformational change of the B2AR biosensor allows the subsequent interaction with its C-terminal sequence derived from Gαs. This increases the efficiency of FRET between CFP and YFP (Figure 1a); thus, the real-time B2AR activity can be monitored by detecting FRET levels. While reporting the activation status of B2AR, the B2AR FRET biosensor is designed not to induce additional activation of the endogenous Gαs signaling pathway, because the activated B2AR in the biosensor prefers to interact with its C-terminal residues, which do not initiate the Gαs signaling event. To further improve the distribution of the biosensor at plasma membrane, a cleavable signal peptide sequence from hemagglutinin (HA)[30] was inserted into the N-terminus of the B2AR biosensor (Figure S1).

Upon the treatment of an agonist isoproterenol (Iso), the B2AR FRET biosensor reports an increase of the FRET/CFP emission ratio within a minute (Figure 1b), suggesting a rapid B2AR activation at plasma membrane as previously reported.[33−35] This B2AR activation at plasma membrane was not detected by a negative control biosensor, which missed the C-terminal Gαs sequence (B2AR-No biosensor) (Figure 1c), confirming that the FRET response is due to the intramolecular interaction between the activated B2AR and the C-terminal sequence derived from Gαs.[26]

Interestingly, after 5 min, the FRET ratio of the B2AR biosensor increased again, with a concomitant appearance of internalized endosomal vesicles (Figure 1d,e). The FRET/CFP level of the biosensor at these newly appeared endosomal vesicles is relatively higher than the nearby region of plasma membrane (Figure 1d). These results suggest that the activated B2AR at plasma membrane is internalized in a few minutes and maintains its activity at the endosomal vesicles, consistent with

https://dx.doi.org/10.1021/acs.analchem.0c03323
Anal. Chem. 2021, 93, 2010−2017

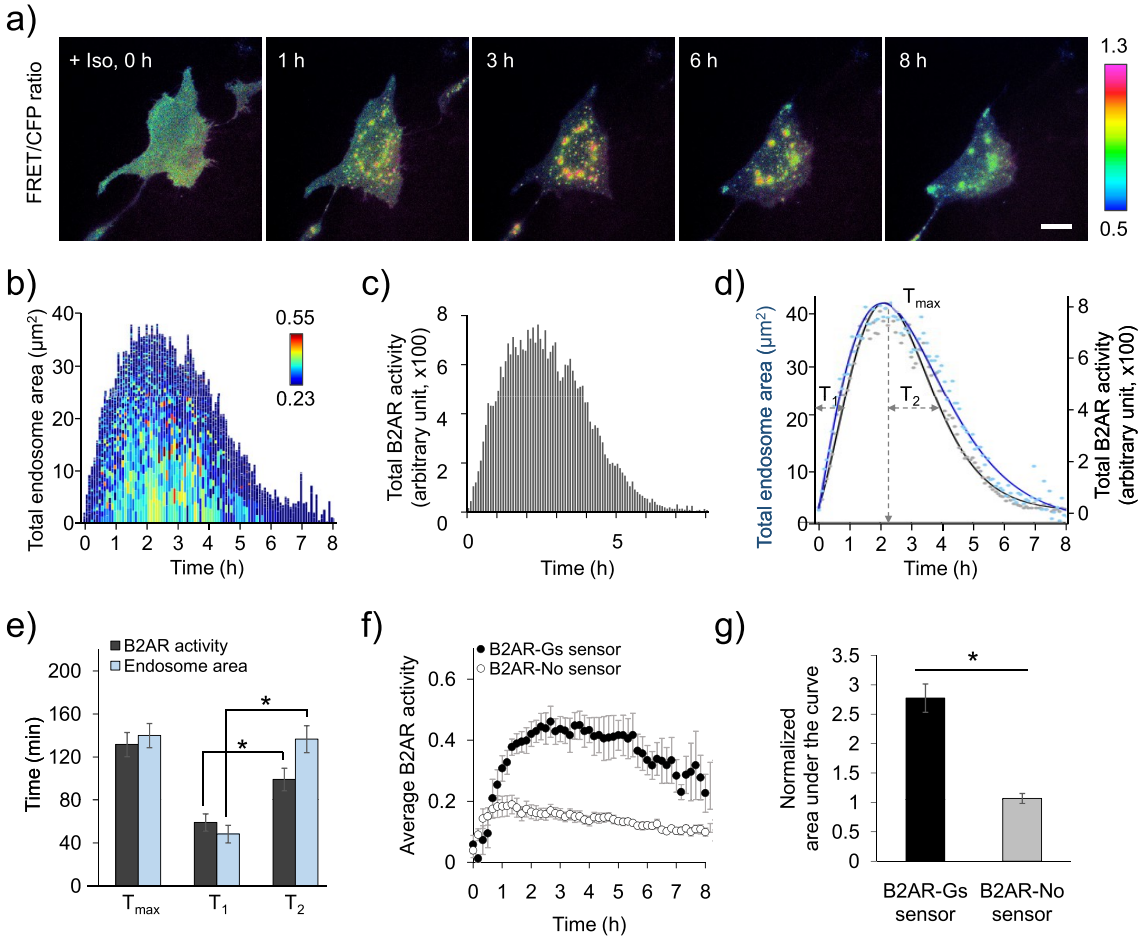

Figure 2. Temporal kinetics of an agonist-induced B2AR activity at the internalized endosomes is explained by a modified Ricker model. (a) FRET/CFP ratio images of the B2AR biosensor after the Iso treatment for indicated times. The rainbow color bar on the right represents the level of FRET/CFP emission ratio. Scale bar, 20 μm. (b) Total endosome area over time after the Iso treatment. Individual B2AR-containing endosome is displayed as a bar, representing its size and FRET level by the length and the rainbow color, respectively. The bars at each time point are sorted by size and further stacked to quantify the total endosome area and the general B2AR activity over time. (c) Total vesicular B2AR activity at each time calculated by the summation of the individual endosomal B2AR activity, which is achieved by multiplication of individual endosome size and its average FRET level. (d) Fitting graph of total endosome area (blue, R^2 = 0.9841) and total B2AR activity at endosomes (gray, R^2 = 0.9866) to new population model inspired from the Ricker model. T_{max} represents the time to reach the maximum B2AR activity; T_1 and T_2 indicate the times to reach the half value in the increasing and decreasing phases. (e) Calculated average values of T_{max}, T_1, and T_2 for total B2AR activity and total endosome area. Data represent the mean value ± s.e.m. of each group experiment (n = 6). * represents significant difference between groups (p = 0.048 and 0.002). (f–g) Average B2AR activity at each time point detected by B2AR-Gs biosensor (n = 7) or B2AR-No biosensor (n = 5) (f), and the area under the curve of B2AR-Gs biosensor normalized by the one of B2AR-No biosensor (g). Data represent the mean value ± s.e.m and * represents significant difference between groups (p = 0.0002).

a previous report.[12] The negative control biosensor can also be internalized upon the Iso treatment but did not show any detectable FRET change (Figures S2a and 1e), suggesting that the FRET response of the B2AR biosensor is not simply due to the accumulation at endosomal vesicles but reporting B2AR activity.

Temporal Kinetics of Endosomal B2AR Activity Is Explained by a Modified Ricker Model. The whole process of B2AR endosomal trafficking pathway (Figure S2b) is suggested to be in the range of several hours;[21−24] thus, we set up a live-cell imaging system for long-term monitoring of the B2AR FRET biosensor in a CO_2 and temperature-controlled chamber. In this system, we can successfully monitor the distribution as well as the dynamic FRET changes of B2AR biosensor-containing endosomes for several hours in live cells (Figure 2a and Video S1). The whole-cell analysis of normalized FRET/CFP ratio revealed an agonist-induced B2AR activation and deactivation for 8 h, while no FRET change was detected without the Iso treatment or by a negative control biosensor (Figure S3). Interestingly, small endosomes, which appeared throughout the whole cell area in an hour, are combined to become bigger vesicles at perinuclear regions at around 2−3 h (Figure 2a and Video S1). It has been suggested that early endosomes are fused to multivesicular endosomes (MVEs),[36] which then further fuse to lysosomes at perinuclear regions.[37] Indeed, after 3 h, both the size and number of B2AR-containing endosomes decrease until 8 h (Figure 2a), possibly indicating the long-term desensitization of B2AR.

To more accurately analyze the B2AR activity at individual endosomes, we developed an automatic vesicle-tracking algorithm (Figure S4). This program identifies individual B2AR-containing endosomes from the CFP images based on the watershed algorithm (Video S2),[31,38] and then calculates the size and the level of the FRET/CFP ratio of the endosome.

https://dx.doi.org/10.1021/acs.analchem.0c03323
Anal. Chem. 2021, 93, 2010−2017

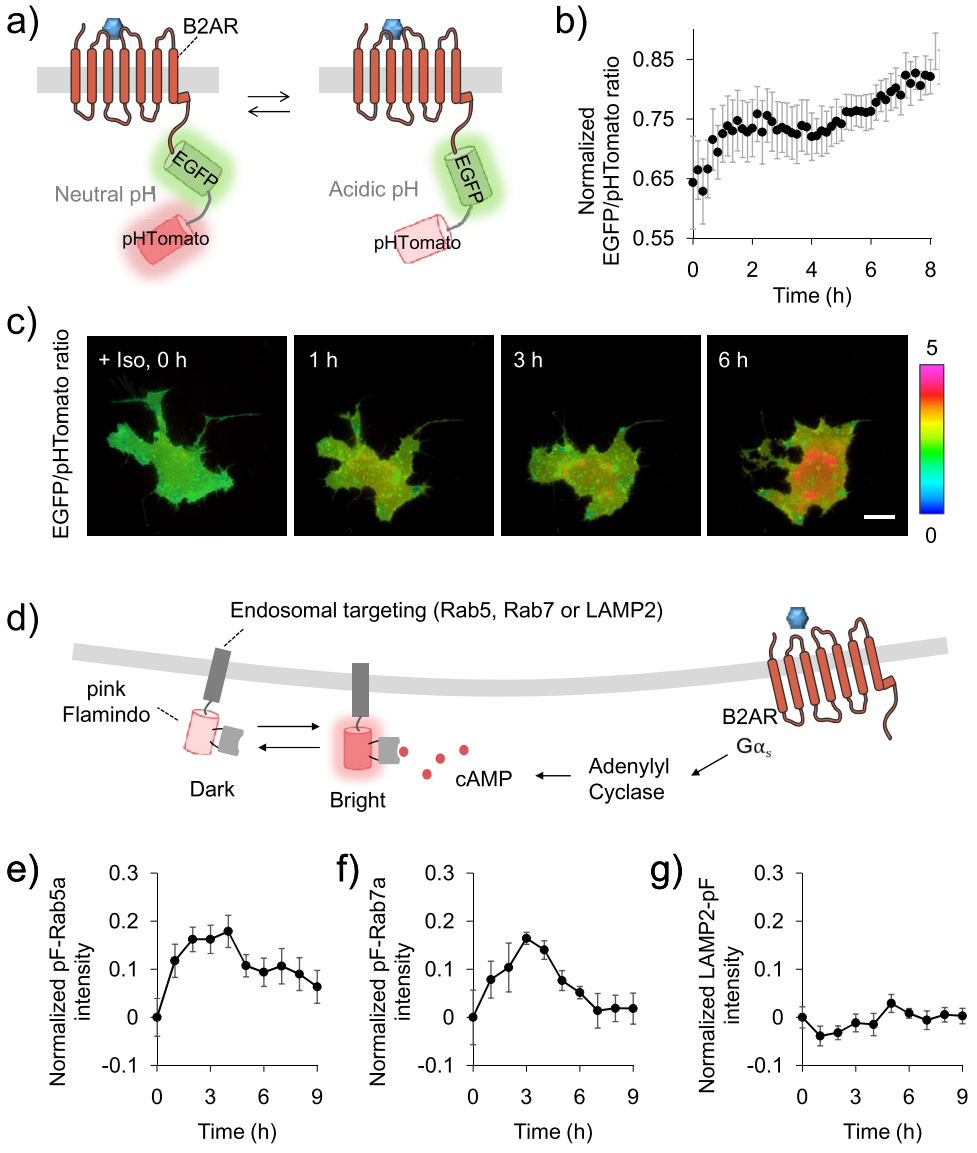

Figure 3. B2AR-induced local cAMP production at different stages of endosomes. (a) Scheme of the B2AR-pH sensitive biosensor containing EGFP and pHTomato. (b, c) Time-lapse values ± s.e.m. (b) and images of the EGFP/pHTomato ratio (c) after the Iso treatment (n = 8). The rainbow bar on the right represents the level of EGFP/pHTomato ratios. (d) Scheme of subcellular targeted pink flamindo (pF) to detect local cAMP production at different stages of endosomes, which is induced by activated B2AR and adenylyl cyclase. (e–g) Time courses of the normalized intensity of pF-Rab5a (n = 4) (e), pF-Rab7a (n = 5) (f), and LAMP2-pF (n = 10) (g) after the Iso treatment. The pF intensity of each cell was normalized by its maximal intensity as 1, and the average data of each group was subtracted by the basal level at time 0. Data represent the mean value ± s.e.m.

At each time point, individual B2AR-containing endosome is displayed as a bar, representing its size and FRET level by the length and the rainbow color, respectively (Figure 2b). These bars at different time points were sorted by size and stacked to quantify the total endosome area as well as the general B2AR activity over time (Figure 2b). The relative change of the total endosome area over time in a single cell indicates the progression stages of the endosomal trafficking pathway.[37] The analysis revealed that the total vesicle area peaks at around 2 h, and the activated B2AR represented by yellow-green color sustained until around 4 h. Then, the endosomal populations containing active B2AR gradually disappear until around 8 h.

The B2AR activity of individual vesicles was calculated by multiplying their size and the FRET level, and the total B2AR activity at each time point was calculated by the sum of the B2AR activity of individual vesicles (Figure 2c). The total B2AR activity at the internalized vesicles increases in 2 h and then decreases to the basal level until around 6 h (Figure 2c). The increasing phases of endosome population and total B2AR activity take around 2 h, but the decreasing phase of the B2AR activity is faster than the endosome population kinetics (Figure 2b,c), suggesting that the activity of B2AR decreases before its complete degradation.

As the internalized B2AR is located at endosomes maintaining its activity, the kinetics of the B2AR activity during the endosomal trafficking pathway may be closely related to the active B2AR-containing endosomal population. Thus, we further investigated whether the B2AR activity kinetics can be explained by a mathematical population model. After various linear and nonlinear (exponential) models were tested, we modified the equation of Ricker model[39] as follows, to compute the total area of the endosomal population (Figure

https://dx.doi.org/10.1021/acs.analchem.0c03323
Anal. Chem. 2021, 93, 2010−2017

2d, blue, R^2 = 0.9841). As expected, our model is also well fitted to the kinetics of endosomal B2AR activity (Figure 2d, gray, R^2 = 0.9866).

$$a_{t+1} = a_t \times c \times \left(1 + \frac{1}{t}\right)^{\alpha} \times e^{r\left(1-\frac{A_t}{k}\right)} \quad (2)$$

when $t \geq 0$, $A_t = \sum_{i=1}^{t} a_i$, $c \leq 1$ and a_0 is a constant.

In eq 2, a_t is the B2AR activity at endosomes measured by FRET at time step t (the current generation); A_t is the total B2AR activity at endosomes up to step t; k is the activation capacity; c is the discount rate; and r is the intrinsic growth rate. Our activation dynamics model predicts the level of active endosomal vesicles in the next generation (a_{t+1}) with the level of the previous generation (a_t) with an intrinsic parameter to adjust the scale (r) and the total accumulated activations (A_t) divided by the activation capacity (k). The magnitude of B2AR activation increases until it reaches the activation capacity and then decreases afterward because the resource needed for new activation is exhausted and its degradation process is started.

Our GPCR activity kinetics model is modified from the Ricker model,[39] represented as $a_{t+1} = a_t \cdot e^{r(1-a_t/k)}$, in that the population of the next generation (a_{t+1}) is predicted from the population of the current generation (a_t) with an intrinsic growth rate and the limited resources. Similarly, in our model, the population of activated B2AR-containing endosomes at the next time point (a_{t+1}) is predicted from the current population (a_t). The intrinsic growth rate of the population may be determined, positively by the strength of the stimulation and negatively by endosome maturation and degradation pathway.

From the fitting curve shown in Figure 2d, we can calculate the kinetic factors: T_{max}, the time to reach the maximum B2AR activity or endosomal population, and T_1 and T_2, the times to reach the half value in the increasing and decreasing phases, respectively. As shown by T_1 and T_2, the decreasing phase is slower than the increasing phase (Figure 2e), implying that the long-term desensitization is generally slower than the B2AR activation process. In addition, the increasing phases (T_1) of B2AR activity and endosome population are very similar, but the decreasing phase (T_2) of B2AR activity is about 40 min faster than endosome population (Figure 2d,e). Indeed, the endosomes containing active B2AR displayed by yellow-green color disappear at around 4 h, while the endosomal population with blue color is observed until 7−8 h (Figure 2b). When we further calculated the average B2AR activity per endosome area, the average B2AR activity sharply decreases after 4 h (Figure 2f). These results suggest that the activity of B2AR decreases earlier than its complete degradation at lysosomes. No FRET change was detected by the negative control biosensor (Figure 2f,g).

Spatial Distribution of the B2AR-Mediated cAMP Production during Trafficking Pathway. During the endosome maturation process, the internal pH becomes more acidic;[37] thus, the trafficking stages of B2AR-containing endosomes can be visualized in live cells by detecting the changes of endosomal pH. Thus, we generated a B2AR-pH sensor by replacing the FRET pair FPs with a pH-sensitive pHTomato and a reference EGFP (Figure 3a). The fluorescence of a pH-sensitive FP, but not a reference FP, will markedly decrease at acidic pH;[40] thus, the intensity ratio of EGFP/pHTomato can report the acidity of the B2AR-containing endosomes. Indeed, after the Iso treatment, the B2AR-pH sensors visualize the acidification process of the B2AR-containing endosomes (Figure 3b,c). In particular, the acidification is accelerated after 4 h, suggesting that B2AR is located inside acidic environments such as late endosomes and lysosomes. Consistently, we observed that the average B2AR activity also decreases after 4 h (Figure 2f).

Finally, we investigated how spatiotemporal B2AR activity mediates the production of cAMP during the endosomal trafficking pathway. We first confirmed that B2AR is trafficked from early endosomes, late endosomes, and then lysosomes by checking the co-localization of the B2AR biosensor with different endosomal markers (Figure S5). To detect the local dynamic changes of cAMP level in live cells, a genetically encoded cAMP indicator, pink Flamindo (pF)[29] was further fused to different endosomal markers, generating pF-Rab5, pF-Rab7a, and LAMP2-pF (Figure 3d). Upon the agonist-stimulated B2AR activation, pF-Rab5 reports an immediate increase in cAMP levels that peaked at 2−3 h, followed by a rapid decrease (Figure 3e), indicating B2AR function at early endosomes. pF-Rab7a tethered at late endosomes shows relatively slower but still increase of cAMP for a longer duration until 3−5 h (Figure 3f). In contrast, no cAMP level was detected by pF-LAMP2 at lysosomes (Figure 3g). These results confirm that during the endosomal trafficking pathway, active B2AR sequentially induces its downstream function following its trafficking pathway for several hours before its degradation at lysosomes.

CONCLUSIONS

In summary, we characterized the spatiotemporal kinetics of the agonist-induced B2AR activation, from a rapid activation at plasma membrane to the long-term desensitization, throughout the endosomal trafficking pathway. Utilizing the FRET-based GPCR biosensor and cAMP indicators targeted at different stages of endosomes, we learned that the B2AR activity is sustained at the internalized endosomes and maintains cAMP production for several hours before its long-term desensitization. Our analysis program allowed us to accurately measure the real-time GPCR activity and its downstream function at the level of individual endosomes. In particular, our experimental data of B2AR activity at the internalized endosomes is well fitted to the new active-vesicle population model. As the spatiotemporal kinetics of GPCR activity is critical for the duration, potency, and functions, our systems can be further utilized to investigate other GPCRs as well as various ligands.

ASSOCIATED CONTENT

Supporting Information

The Supporting Information is available free of charge at https://pubs.acs.org/doi/10.1021/acs.analchem.0c03323.

Improved distribution of the FRET-based B2AR biosensor (Figure S1); representative images of internalized B2AR-Gs and B2AR-No biosensors (Figure S2a); scheme of endosomal trafficking pathway (Figure S2b); time-lapse changes of the FRET/CFP ratios in the cells expressing B2AR-Gs or B2AR-No biosensors with or without the treatment of Isoproterenol (Figures S3); flow chart of the vesicle analysis program (Figure S4); the sequential co-localization of B2AR biosensor with the markers for endosomal trafficking pathway, EEA-1, Rab7a and LAMP-1 (Figure S5); the sequence information of B2AR biosensor, B2AR-pH sensor, pF-Rab5a, pF-Rab7a and LAMP2-pF (Figure S6) (PDF)

https://dx.doi.org/10.1021/acs.analchem.0c03323
Anal. Chem. 2021, 93, 2010−2017

Time-lapse imaging of B2AR FRET biosensor in response to the Iso treatment (MP4)
Automatic vesicle detection by vesicle-tracker (MP4)

AUTHOR INFORMATION

Corresponding Authors

Jaesik Choi − *Graduate School of Artificial Intelligence, Korea Advanced Institute of Science and Technology (KAIST), Daejeon 34141, Republic of Korea*; Email: jaesik.choi@kaist.re.kr

Jihye Seong − *Brain Science Institute, Korea Institute of Science and Technology (KIST), Seoul 02792, Republic of Korea; Department of Converging Science and Technology, Kyung Hee University, Seoul 02447, Republic of Korea*; orcid.org/0000-0001-8450-3315; Email: jseong@kist.re.kr

Authors

Hyunbin Kim − *Brain Science Institute, Korea Institute of Science and Technology (KIST), Seoul 02792, Republic of Korea; Division of Bio-Medical Science & Technology, KIST School, Korea University of Science and Technology, Seoul 02792, Republic of Korea*

Hae Nim Lee − *Brain Science Institute, Korea Institute of Science and Technology (KIST), Seoul 02792, Republic of Korea; Department of Converging Science and Technology, Kyung Hee University, Seoul 02447, Republic of Korea*

Complete contact information is available at: https://pubs.acs.org/10.1021/acs.analchem.0c03323

Notes

The authors declare the following competing financial interest(s): J.S. and H.K. are inventors of vesicle analysis program.

ACKNOWLEDGMENTS

This work is supported in part by the Brain Research Program through the National Research Foundation of Korea (NRF) (2017M3C7A1043842), the National Research Council of Science & Technology (NST) grant by the Korea government (No. CRC-15-04-KIST), KIST Institutional Grant 2E30963 and Samsung Research Funding & Incubation Center of Samsung Electronics under Project Number SRFC-TC2003-02 (J.S.). This work is also supported by the Institute for Information and Communications Technology Planning and Evaluation (IITP) grants funded by the Korea government (2017-0-01779 and 2019-0-00075) (J.C.).

REFERENCES

(1) Cerione, R. A.; Codina, J.; Benovic, J. L.; Lefkowitz, R. J.; Birnbaumer, L.; Caron, M. G. *Biochemistry* **1984**, *23*, 4519−4525.
(2) Rosenbaum, D. M.; Rasmussen, S. G.; Kobilka, B. K. *Nature* **2009**, *459*, 356−363.
(3) Krupnick, J. G.; Benovic, J. L. *Annu. Rev. Pharmacol. Toxicol.* **1998**, *38*, 289−319.
(4) Moore, C. A.; Milano, S. K.; Benovic, J. L. *Annu. Rev. Physiol.* **2007**, *69*, 451−482.
(5) Luttrell, L. M.; Lefkowitz, R. J. *J. Cell Sci.* **2002**, *115*, 455−465.
(6) Eichel, K.; von Zastrow, M. *Trends Pharmacol. Sci.* **2018**, *39*, 200−208.
(7) Vilardaga, J. P.; Jean-Alphonse, F. G.; Gardella, T. J. *Nat. Chem. Biol.* **2014**, *10*, 700−706.
(8) Sposini, S.; Hanyaloglu, A. C. *Prog. Mol. Subcell. Biol.* **2018**, *57*, 273−299.
(9) Calebiro, D.; Nikolaev, V. O.; Gagliani, M. C.; de Filippis, T.; Dees, C.; Tacchetti, C.; Persani, L.; Lohse, M. J. *PLoS Biol.* **2009**, *7*, No. e1000172.
(10) Ferrandon, S.; Feinstein, T. N.; Castro, M.; Wang, B.; Bouley, R.; Potts, J. T.; Gardella, T. J.; Vilardaga, J. P. *Nat. Chem. Biol.* **2009**, *5*, 734−742.
(11) Mullershausen, F.; Zecri, F.; Cetin, C.; Billich, A.; Guerini, D.; Seuwen, K. *Nat. Chem. Biol.* **2009**, *5*, 428−434.
(12) Irannejad, R.; Tomshine, J. C.; Tomshine, J. R.; Chevalier, M.; Mahoney, J. P.; Steyaert, J.; Rasmussen, S. G.; Sunahara, R. K.; El-Samad, H.; Huang, B.; von Zastrow, M. *Nature* **2013**, *495*, 534−538.
(13) Kuna, R. S.; Girada, S. B.; Asalla, S.; Vallentyne, J.; Maddika, S.; Patterson, J. T.; Smiley, D. L.; DiMarchi, R. D.; Mitra, P. *Am. J. Physiol.: Endocrinol. Metab.* **2013**, *305*, E161−E170.
(14) Feinstein, T. N.; Yui, N.; Webber, M. J.; Wehbi, V. L.; Stevenson, H. P.; King, J. D., Jr.; Hallows, K. R.; Brown, D.; Bouley, R.; Vilardaga, J. P. *J. Biol. Chem.* **2013**, *288*, 27849−27860.
(15) Tsvetanova, N. G.; von Zastrow, M. *Nat. Chem. Biol.* **2014**, *10*, 1061−1065.
(16) Musheshe, N.; Schmidt, M.; Zaccolo, M. *Trends Pharmacol. Sci.* **2018**, *39*, 209−222.
(17) Lazar, A. M.; Irannejad, R.; Baldwin, T. A.; Sundaram, A. B.; Gutkind, J. S.; Inoue, A.; Dessauer, C. W.; Von Zastrow, M. *Elife* **2020**, *9*, No. e58039.
(18) Pavlos, N. J.; Friedman, P. A. *Trends Endocrinol. Metab.* **2017**, *28*, 213−226.
(19) Rajagopal, S.; Shenoy, S. K. *Cell. Signalling* **2018**, *41*, 9−16.
(20) Tsao, P.; Cao, T.; von Zastrow, M. *Trends Pharmacol. Sci.* **2001**, *22*, 91−96.
(21) Shenoy, S. K.; McDonald, P. H.; Kohout, T. A.; Lefkowitz, R. J. *Science* **2001**, *294*, 1307−1313.
(22) Whistler, J. L.; Enquist, J.; Marley, A.; Fong, J.; Gladher, F.; Tsuruda, P.; Murray, S. R.; Von Zastrow, M. *Science* **2002**, *297*, 615−620.
(23) Simonin, F.; Karcher, P.; Boeuf, J. J.; Matifas, A.; Kieffer, B. L. *J. Neurochem.* **2004**, *89*, 766−775.
(24) Marchese, A.; Paing, M. M.; Temple, B. R.; Trejo, J. *Annu. Rev. Pharmacol. Toxicol.* **2008**, *48*, 601−629.
(25) Lobingier, B. T.; von Zastrow, M. *Traffic* **2019**, *20*, 130−136.
(26) Malik, R. U.; Ritt, M.; DeVree, B. T.; Neubig, R. R.; Sunahara, R. K.; Sivaramakrishnan, S. *J. Biol. Chem.* **2013**, *288*, 17167−17178.
(27) Hall, R. A.; Premont, R. T.; Chow, C. W.; Blitzer, J. T.; Pitcher, J. A.; Claing, A.; Stoffel, R. H.; Barak, L. S.; Shenolikar, S.; Weinman, E. J.; Grinstein, S.; Lefkowitz, R. J. *Nature* **1998**, *392*, 626−630.
(28) Cao, T. T.; Deacon, H. W.; Reczek, D.; Bretscher, A.; von Zastrow, M. *Nature* **1999**, *401*, 286−290.
(29) Harada, K.; Ito, M.; Wang, X.; Tanaka, M.; Wongso, D.; Konno, A.; Hirai, H.; Hirase, H.; Tsuboi, T.; Kitaguchi, T. *Sci. Rep.* **2017**, *7*, No. 7351.
(30) Guan, X. M.; Kobilka, T. S.; Kobilka, B. K. *J. Biol. Chem.* **1992**, *267*, 21995−21998.
(31) Bradski, G. *Dr. Dobb's Journal of Software Tools* **2000**, *120*, 122−125.
(32) Abadi, M.; Agarwal, A.; Barham, P.; Brevdo, E.; Chen, Z.; Citro, C.; Corrado, Gs.; Davis, A.; Dean, J.; Devin, M.; Ghemawat, S.; Goodfellow, I.; Harp, A.; Irving, G.; Isard, M.; Jia, Y.; Kaiser, L.; Kudlur, M.; Levenberg, J.; Zheng, X. In *TensorFlow: Large-Scale Machine Learning on Heterogeneous Distributed Systems*, Proceedings of the 12th USENIX conference on Operating Systems Design and Impelementation, 2016; pp 265−283.
(33) Vilardaga, J. P.; Bunemann, M.; Feinstein, T. N.; Lambert, N.; Nikolaev, V. O.; Engelhardt, S.; Lohse, M. J.; Hoffmann, C. *Mol. Endocrinol.* **2009**, *23*, 590−599.
(34) Lohse, M. J.; Bunemann, M.; Hoffmann, C.; Vilardaga, J. P.; Nikolaev, V. O. *Curr. Opin. Pharmacol.* **2007**, *7*, 547−553.
(35) Vilardaga, J. P. *J. Recept. Signal Transduction Res.* **2010**, *30*, 304−312.
(36) Gruenberg, J.; Stenmark, H. *Nat. Rev. Mol. Cell Biol.* **2004**, *5*, 317−323.

(37) Huotari, J.; Helenius, A. *EMBO J.* **2011**, *30*, 3481−3500.
(38) Beucher, S.; Meyer, F. *Math. Morphol. Image Process.* **1993**, *12*, 33−81.
(39) Brännström, Å.; Sumpter, D. J. *Proc. R. Soc. B* **2005**, *272*, 2065−2072.
(40) Li, Y.; Tsien, R. W. *Nat. Neurosci.* **2012**, *15*, 1047−1053.

https://dx.doi.org/10.1021/acs.analchem.0c03323
Anal. Chem. 2021, 93, 2010−2017